IEEE Access
Multidisciplinary ⋮ Rapid Review ⋮ Open Access Journal

Received 6 March 2024, accepted 13 May 2024, date of publication 16 May 2024, date of current version 24 May 2024.

Digital Object Identifier 10.1109/ACCESS.2024.3402112

RESEARCH ARTICLE

Increasing the Fitting Precision of Implicit Polynomial Curves in 2D Modeling Through Signomial Powers

IHSAN PENCE
Department of Software Engineering, Burdur Mehmet Akif Ersoy University, 15300 Burdur, Turkey
e-mail: ihsanpence@mehmetakif.edu.tr

ABSTRACT Today, common algorithms such as spline curves and triangulation methods are used in 2-and 3-dimensional modeling of objects. However, although these methods can express objects well in terms of visuality because they treat objects as a combination of many small parts, they cannot reveal the mathematical expression of the whole object. The most prominent method of expressing objects with a single equation is the implicit polynomial (IP) curves and the 3L method used to realize the more precise effects of these curves. In this study, the 3L method was accepted as the primary method, and signomial functions using real number powers were used to increase the fitting precision in 2D modeling. The artificial bee colony (ABC) algorithm was used to determine signomial terms. Based on the root mean square error, peak signal-to-noise ratio, coefficient of determination, and structural similarity values obtained in experimental studies, modeling success can be increased. Also, due to adding the initial power expression of IP as the population element for ABC, the sensitivity of the current IP model is increased rather than remodeled.

INDEX TERMS Signomial functions, implicit polynomial curves, 3L method, artificial bee colony, modeling.

I. INTRODUCTION

Polynomial curves or surfaces have many advantages, allowing them to be preferred in computerized vision studies. Complex objects that do not have simple geometric shapes, such as squares and circles, are difficult to represent with simple ellipse curves. Such complex objects and shapes can be better modeled with high-degree curves or surfaces. These models are noise-resistant and capable of modeling at reasonable levels for missing data. In addition, point classification problems and curve-surface intersection calculations can only be performed with a simple polynomial expression.

Although common algorithms such as spline curves and triangulation methods are used for modeling today, these methods do not fully express the mathematical equation that covers the entire model. For this reason, modeling any shape or object is among the issues that have not yet been resolved in the literature. Among the methods that can express objects as a whole, the most prominent one is Implicit Polynomial (IP) curve. This curve is also available in methods such as 3L, which can model this curve more precisely. Besides these, parametric curves need extra parameters besides the data's coordinate plane variables. Because of its advantages, such as general shape representation of the object, smoothing noisy data, and resistance to occlusion, IP is more suitable for data fitting algebraic curves than parametric curves.

IP and polynomial curves fail in high-precision modeling because the degrees of power are integers, even though they can mathematically express objects or shapes. Although methods such as 3L are used to increase success with these methods, the only option for more precise modeling is by increasing the degree of power. The increase in the degree of power increases the number of terms in mathematical expression, and this is not desirable in terms of memory savings and complexity. High memory usage and delays occur due to excessive terms when recreating equations of

The associate editor coordinating the review of this manuscript and approving it for publication was Songwen Pei.

modeled objects in various games or drawing programs. This is undesirable for systems that operate in real-time. When it is thought that equations of objects can be used in real-time systems such as games or animation, it is preferable to have better results in the number of terms available instead of increasing the number of terms in the equation. This study suggests that using signomial and posynomial functions with real power degrees can increase modeling sensitivity for the same number of terms.

When the studies carried out in the literature are analyzed, it is seen that while IP and 3L methods are often used in image processing applications, signomial functions are often used in optimization problems. Their applications in image processing are relatively limited. The advancement of IP applications in the field of image processing was accelerated by the work of Taubin [1], while the 3L algorithm was developed by Lei et al. [2]. Later, Blane developed implicit surfaces using the 3L algorithm for various two-and three-dimensional (3D) data [3]. Among the studies conducted with implicit curves and surfaces, there are studies, in which implicit curves are used for ellipses modeling [4], it is checked whether perspective or parallel projection matching for rational and implicit curves is seen or not [5], an algorithm that draws 3D graphics of implicit functions of three variables is developed [6], sampling, reconstruction and limits are designated by using implicit polynomial curves over the binary images [7], rational implicit polynomial are used for complex figures [8], parabolic, ridge and sub-parabolic curves are analysed on the implicit surfaces defined with smooth functions [9], 3D figures are reconstructed with implicit polynomial curves [10], optimum implicit polynomial is designated with 3L method and algebraic surface adaptation in order to model deformation on 3D surfaces [11], an implicit form is obtained for a canal surface whose spine is a spring and radius changes as linear according to angle [12], an algorithm that can designate the geometrical distance of a point in 3D space to the implicit curve is proposed [13], a new compression algorithm is proposed for coefficient tensors for implicit 3D B-spline solids [14]. IP and 3L algorithms have been employed in other studies in modeling [15], [16], [17], [18], [19], [20], [21], [22], [23], [24].

In addition to these studies, applications are carried out with different methods for different purposes. Besides studies based on radial basis function using offset points [25], studies based on Hermite radial basis function not using offset points are also available [26], [27]. In the literature, there are also other studies in which noise is prevented on 2-dimensional (2D) infrared images with wavelet filter and background image is cleaned from infrared image by composing 3L+1 layered sub-images [28], the undecimated wavelet transform and grey level co-occurrence matrix are combined in order to obtain detailed textural specifications on the mammogram images [29], it is shown that free-form curves with properly defined essential functions are the solution curves of linear differential systems [30], implicit curves and surfaces are reconstructed from point cloud by using Gaussian Radial basis functions [31], a new image modeling is developed by combining boundary representation and parametrical methods [32], boundary images defined as unstable are modeled by using parametrical integral equations system [33], the aluminum grain boundary of the ellipsoid and quadratic surfaces the tessellation process is performed based on the 3D pictures can be fabricated with [34], the exponential representation of the curves and classical linear differential systems modeling are compared [35].

Duffin et al. introduced signomial functions [36]. Studies have shown that these functions using real number powers are generally considered to be optimization problems in the literature and to be solved by geometric programming and global optimization techniques [37], [38], [39], [40], [41]. The application of signomial functions is quite rare in the field of image processing and modeling; some studies renovate and reconstruct the double and grayed-out pictures by using signomial programming [42], in which noisy pictures are cleaned by using Fourier transform and signomial functions [43], equations with real number power can be expressed mathematically [44], signomial programming is used for the most suitable aircraft model design [45], [46], [47], error definition with non-integer exponents for the linear axis [48], and the fractional polynomial method is used to evaluate the system performance [49]. Additionally, studies in which polynomial coefficients are determined by deep learning to find the 2D image boundary line include [50] for IPs and [51] for fractional implicit polynomials.

The studies in the literature employ implicit curves/surfaces and optimization techniques together are minimal. Interian et al. (2017) attempted to determine the degree of polynomials that should be used to model 2D and 3D images with IP through particle swarm optimization (PSO) and differential evolution (DE) algorithms, which are heuristic methods. The value determined in the relevant study is the degree of IP number that should be used [52].

A comparative analysis of signomial functions in image processing and modeling applications is given in Table 1.

In Table 1, although it can be determined by various methods that the number of IP should be used in the studies given in the literature, the powers of each term have not been dealt with individually. This study focused on the combination of signomial modeling and heuristic optimization in image modeling and increased the fitting precision in 2D modeling to the same degree. The 3L method was preferred as the basic algorithm because it can successfully model 2D shapes and 3D objects. As an experimental study, some 2D figures in the literature were modeled with IP and signomial functions. Modeling was carried out by incorporating the 3L method into IP and signomial functions. Although the shapes were modeled meaningfully using the 3L method with IP, signomial functions were necessary to enhance sensitivity. In this study, the expression, as much as the number of terms formed due to the degree of power determined for IP, was

TABLE 1. The literature comparison of signomial functions in image processing and modeling.

Study	Method	Usage	Objective
Shen et al. (2008) [42]	Signomial programming	Penalizing least-squares	Image restoration
Zhang and Ye (2011) [43]	Fast Fourier transform	Penalizing least-squares	Image restoration
Cetisli and Kalkan (2011) [44]	Genetic algorithm	Determining real powers	Curve fitting
Kirschen et al. (2016) [45]	Signomial programming	Optimizing a configuration	Aircraft design
Interian et al. (2017) [52]	PSO and DE	Finding the degree of IP	2D/3D image fitting
Kirschen et al. (2018) [46]	Signomial programming	Optimizing a configuration	Aircraft design
Xu et al. (2020) [48]	Non-integer exponent function	Pre-fitting the errors	Identifying errors for machine tools
Öztürk and Saab (2021) [47]	Signomial programming	Optimizing a configuration	Aircraft design
Zhou et al. (2021) [49]	Fractional polynomial	Determining fractional powers	Describing system reliability
Wang et al. (2022) [50]	Deep learning based Encoder-X	Determining IP coefficients	2D image fitting
Tong et al. (2023) [51]	Deep learning based TSEncoder	Determining fractional IP coefficients	2D image fitting
Proposed Method	ABC	Determining real powers	2D image fitting

modeled by the real number powers of signomial functions. The Artificial Bee Colony (ABC) algorithm [53], a heuristic method, was employed to determine the real power degrees of the signomial function. As a result of adding the initial power expression of IP as a population element for ABC, the sensitivity of the existing model was increased rather than undergoing remodeling.

The novelty and contribution are: (i) for the first time, an attempt is made to increase the fitting precision of 2D shapes by using signomial powers together with the 3L method; (ii) with this approach, more precise modeling can be performed without increasing the number of terms in the mathematical model.

This study is organized as follows: the first part discusses the importance of implicit modeling and relevant studies, the second part mentions the materials and methods as well as explains the dataset and methods, the third part includes experimental studies and optimizing of signomial powers, and the final part includes the conclusions.

II. MATERIALS AND METHODS

This study used boots, aircraft, cells, pliers, and guitars from 2D shapes included in the literature as data sets to test modeling success. These 2D shapes, which are mostly not publicly available data sets [50], form the target curves of IP. In this study, hand drawings with a curved structure were used in modeling, where the success of fitting precision could be better determined. Other reasons for preferring hand drawings as a data set are that these images provide data diversity by covering noisy examples in the real world, can improve the model's generalization ability, and can reduce the overfitting problem. Draft drawings are provided in Supplementary files.

Different images in the dataset may require different polynomial degrees for optimal representation due to their unique characteristics. Complex images may require higher-degree polynomials for accurate modeling, while lower-degree polynomials may be sufficient for images with more superficial structures. This study employed polynomial powers that could effectively model images with diverse structures at a visually acceptable level. For this reason, different degrees were utilized for each image. Higher polynomial degrees were used, especially in some complex images, because curved structures could not be modeled at the desired level. Since hand drawings were used in this study, the data set also contains slight noise. The use of higher-degree polynomials may result in overfitting, especially in less complex data sets, and may cause noise to be included in the model.

In the field of modeling, normalization processes are frequently employed to express the object in a standard format. The result obtained in many normalization methods reduces the adverse effects of the implicit algebraic curve. This usually occurs more in higher-degree polynomials. In high-degree polynomials, the noise-like corresponding impact increases in the ratio of the degree of power. The radial distance normalization method was used in this study. The normalized data was then divided into layers using the 3L algorithm for modeling performance. IP and signomial functions were used to find the power values of the layered data, and the real number powers of the signomial function were found by ABC, one of the popular heuristic methods in the literature. Finally, to identify the coefficients of both IP and signomial expressions, the ridge regression method was employed in the modeling process. This method has the potential to distort unwanted excess curves.

A. IMPLICIT ALGEBRAIC CURVES

All linear implicit curve fitting techniques aim to converge the given data set with the help of a polynomial by minimizing the algebraic distances between them as much as possible. Implicit algebraic curves and optional selected n-degree IP models can be represented in 2D, as shown in Equation (1). The number of coefficients for 2D of the implicit algebraic curve is $c = (n + 1)*(n + 2)/2$.

$$f(x, y) = \sum_{i,j\geq 0, i+j\leq n} a_{ij} x^i y^j = 0 \tag{1}$$

Algebraic curves or surfaces model sample objects by considering the measured geometric data and consequently form the global expression of the object. The (x-y) pairs in Equation (1) that result in the value of the function being equal to zero provide the solution and thereby form the 2D shape.

B. 3L ALGORITHM ON 2-DIMENSIONAL OBJECTS

The 3L algorithm was developed for the first time by Lei et al. [2], and the method is based on the constraint principle to ensure that the fitting polynomial passes through the data and the other two layers. In this way, the fitting polynomial can eliminate the singularity and follow the data environment.

The main idea of the 3L algorithm for shapes is to represent the entire shape by classifying each 2D point as lying outside, inside, or precisely on the shape. Consequently, the curve to be constructed is initially joined with the points at a distance of ε from the inner and outer sides of the original data. The Euclidian distance can be employed to perform this operation. According to the implicit function, it is forced to take the value $+1$ in the outer layer, -1 in the inner level, and 0 in the middle layer. Thus, b as a vector and M as a 3-layer data matrix are expressed in Equation (2) [16].

$$\begin{aligned} \mathrm{b} &= [+1 \ldots +10 \ldots 0 -1 \ldots -1]^{\mathrm{T}}_{(3\mathrm{Nx1})}, \\ \mathrm{M} &= \begin{bmatrix} \mathrm{M}_{+\varepsilon} \\ \mathrm{M}_{0} \\ \mathrm{M}_{-\varepsilon} \end{bmatrix} = \begin{bmatrix} \mathrm{Y}_1^{\mathrm{T}} \\ \mathrm{Y}_2^{\mathrm{T}} \\ \cdots \\ \mathrm{Y}_{3\mathrm{N}}^{\mathrm{T}} \end{bmatrix}_{3\mathrm{Nxc}} \end{aligned} \tag{2}$$

C. RIDGE REGRESSION METHOD

Recently, linear approaches to curve fitting problems have begun to emerge. However, these techniques often fail to provide global stabilization for many situations and are not resistant to disturbing effects such as noise. Several methods have been developed to address these effects, but ridge regression analysis has emerged as a prominent technique. Ridge regression is one of the deviation estimation methods. It is preferred in multicollinear cases because it gives estimates with more minor variance than the variance of the least squares method. The method allows for the inclusion of all variables in the model.

The coefficient vector of the result curve can be obtained by the least squares method, as demonstrated in Equation (3).

$$\mathrm{a_K} = (\mathrm{M^T M})^{-1} \mathrm{M^T b} \tag{3}$$

Linear curve fitting techniques ensure local stability around data points. However, they are inadequate for global stability. The values of the single-term matrix $\mathrm{M^T}$, M in the near multiple connections in the data are approximately singular, as some eigenvalues are much smaller than others. These eigenvalues cannot contribute to fitting the data set around itself and contain extra open, unstable branches. The open, unstable curves around the object are permanently displaced as a result of the ridge regression method, so the term kD in Equation (4) is applied by adding the least squares method [16].

$$\mathrm{a_K} = (\mathrm{M^T M} + \mathrm{kD})^{-1} \mathrm{M^T b} \tag{4}$$

In the ridge regression method, the diagonal D matrix, which has the same number of terms as the $\mathrm{a_K}$ coefficient vector, can be selected as the identity matrix.

D. SIGNOMIAL FUNCTIONS AND ARTIFICIAL BEE COLONY

Unlike polynomials, signomial functions are expressions whose power degree and coefficients can be real numbers. The function is called a posynomial if the coefficient expression is a positive real number [36]. An example signomial expression is presented in Equation (5).

$$\mathrm{f}(\mathrm{x}_1, \mathrm{x}_2, \mathrm{x}_3) = 4.6\mathrm{x}_1^2\mathrm{x}_2^{-0.3}\mathrm{x}_3^{0.7} - 2\mathrm{x}_1^{-4}\mathrm{x}_3^{3.2} \tag{5}$$

In terms of modeling, signomial functions contain real number powers, which enables them to perform precise modeling but may present challenges in calculation. To address this, a heuristic optimization algorithm has been employed to determine the optimal power degrees. In this study, the ABC is used as a heuristic algorithm.

The ABC is based on swarm intelligence and was first proposed by Karaboga [53]. The ABC is one of the most popular heuristic algorithms in the literature and can model the foraging behavior, learning, information sharing, and memorization of bees. The ABC algorithm models the intelligent decision-making behavior of a bee colony that gathers information from an environment and adjusts its behavior accordingly. The model of minimum forage selection that leads to the emergence of collective intelligence consists of three essential components: food sources, attendant worker bees, and non-commissioned worker bees. Bees communicate about the quality of their food sources in the dance area with a waggle dance. The direction and duration of this dance are closely related to the direction and distance of the food source declared by the dancing bee. Worker bees share their knowledge with a probability proportional to the food source's profitability. Scout bees randomly start searching for food sources around the hive. The scout bee that discovers the food source begins to carry nectar from the food source to the hive [53].

To model these behaviors of bees in the computer environment, the ABC algorithm first performs the random determination of the starting positions of the food sources as in Equation (6).

$$\mathrm{x}_{ij} = x_j^{min} + \mathrm{rand}(0, 1)(x_j^{max} - x_j^{min}) \tag{6}$$

In Equation (6), x_j^{min} is the lower bound, x_j^{max} is the upper bound, x_{ij} is the solution vector ($j = 1, 2, \ldots, c$), and $i = 1, 2, \ldots, SN$. Here, c is the number of the parameters, and SN is the number of solutions. Based on their assigned tasks, the ABC algorithm divides bees into three types: worker bees, onlooker bees, and scout bees. Each phase of the worker, onlooker, and scout bees occurs in cycles. Each stage of the process is reviewed to determine the best solution, and the process continues until the stopping criterion has been met. During the worker bee phase, new solutions are generated by examining the neighborhoods of existing solutions,

as in Equation (7).

$$x'_{ij} = x_{ij} + \Phi_{ij}(x_{ij} - x_{kj}) \tag{7}$$

In Equation (7), x' is the new candidate solution vector, Φ_{ij} is a randomly determined number in the range of -1 to 1, and x_k corresponds to a randomly chosen neighbor solution vector. A greedy selection method is then used to compare this new solution to existing solutions. The new solution is used if the new candidate solution is considered better, otherwise the counter is increased. This counter determines whether the food source has been exhausted. A fitness-based probabilistic selection method determines the best solution in the onlooker bee phase. Equation (8) is used to calculate the probability of individuals.

$$P_i = \frac{Fitness_i}{\sum_{i=1}^{SN} Fitness_i} \tag{8}$$

In Equation (8), P_i is the probability value of solution i. After choosing a solution, a greedy selection is applied, much as in the worker bee phase, to keep the better solution for the population. If the solutions do not improve, the counter is increased again. If the trial counter of a solution x_i exceeds the parameter ''limit'', the corresponding source is abandoned. After that, the bee from that source acts as a scout bee. During the scout bee phase, the bees perform a random search [54].

E. PROPOSED ALGORITHM FOR SEARCHING SIGNOMIAL POWERS USING ARTIFICIAL BEE COLONY

This study employs the classical ABC algorithm to find the real number powers of the signomial functions. In general, the ABC algorithm begins with a random initial population, as stated in Equation (6). In the proposed algorithm, the initial population of the ABC algorithm is initialized with IP powers. In this way, worse results than the classical IP method are prevented, and the solution space is improved. The ridge regression method determines the coefficients of the signomial function for which real number powers are sought and determined. The optimal values obtained by the proposed algorithm express the signomial powers, and these powers can be used together with the 3L method. The algorithm for the proposed signomial function is presented in Algorithm (1).

As shown in Algorithm (1), the initial step of the proposed method is to determine c, which represents the number of parameters to be optimized for the signomial function. While the number of coefficients for n-degree IP is calculated with (n+1)∗(n+2)/2, when the powers of the constant term are not taken into account, there are (n+1)∗(n+2)/2-1 power-containing coefficients. There are two powers in each 2D IP (x-y) term containing the coefficient. For this reason, the number c is calculated as ((n+1)∗(n+2)/2-1)∗2 and found as (n+1)∗(n+2)-2. Then, the initial population with c parameters is determined according to Equation (6). The proposed algorithm updates the randomly generated initial population using the known IP powers. For this, the value of x_{1j}, which represents the first population in the solution vector in Equation (6), is replaced with the n-degree IP power given in Equation (1). Then, using the ridge regression method, the coefficients of the signomial function are found according to Equation (4). The resulting signomial function is expressed as M_0 and calculated according to Equation (2) using the 3L algorithm. The objective function value is calculated according to the performance metrics resulting from the 3L algorithm and the original shape. The ABC algorithm minimizes the objective function value and the x_{ij} solution vector is improved. This process is continued for the defined number of iterations. As a result, the optimal values obtained are the powers of the signomial function.

Algorithm 1 Searching for Signomial Powers Using ABC

Begin
Determine c, which is the number of parameters to be optimized for the signomial function using n-dimensional IP terms as (n+1)∗(n + 2) - 2
Create the initial population of the ABC algorithm with c variables
Replace the value of x_1 with the n-degree IP powers given in Equation (1)
while (maximum iteration number is not reached)
    Find coefficients of new populations using Equation (4)
    Calculate objective function values according to Equation (2)
    Determine new populations using the ABC optimization algorithm
end while
Return optimal parameters
End

F. BINARY IMAGES AND PERFORMANCE METRICS

Binary images have only two values (black and white) and can be obtained with the help of existing point clouds or modeled equations in terms of algebraic curves. Binary images can be evaluated with criteria such as similarity and quality with another binary image of the same size. Although IP and ABC algorithms use the 3L method and ridge regression, unwanted branches can still appear on binary images. To perform a performance evaluation between the original image and the modeled image, it is necessary to eliminate the unstable branches. This allows for comparisons to be made on modeled objects alone. This study used Algorithm (2) to clear unstable branches in binary images containing modeled objects.

Performance evaluation could be done with the binary image obtained by Algorithm (2) and the original binary image expressed by M_0 in Equation (2).

Root mean square error (RMSE), peak signal-to-noise ratio (PSNR), coefficient of determination (R^2), and structural similarity (SSIM) metrics were used to evaluate modeling success. These metrics are used to evaluate the similarity and quality of images.

Algorithm 2 Elimination of Unstable Branches on Binary Images

Begin
Input: IP or ABC binary image, which is the sets of (x,y) in Equation (1)
Output: more stable binary image
Labeling of every separate shape on the input image
Calculating the area of every label using their pixels
Determining the label lbl_{max}, which has the maximum area
for i=1:number of labels
  if i $\neq lbl_{max}$
    Eliminate i th label by updating their pixel values to zero
  end if
end for
End

RMSE is a metric that measures the magnitude of the error and is often used to find the distance between the generated model values and the actual values. Equation (9) shows the RMSE calculation of an image in mxn dimensions.

$$RMSE = \sqrt{\frac{1}{mxn}\sum_{i=1}^{m}\sum_{j=1}^{n}\left(I\left(i,j\right)-I'\left(i,j\right)\right)^2} \quad (9)$$

In Equation (9), I indicate the original image while I′ indicate the modeled image.

The PSNR is a metric that indicates the ratio of the maximum possible power of a sign to the power of the noise on the sign. PSNR can be considered an approach to human quality perception and is calculated as in Equation (10).

$$PSNR = 20\log_{10}\left[\frac{1}{RMSE}\right] \quad (10)$$

R^2 is a measure that allows one to determine how certain one can make predictions from a certain model. Equation (11) shows the formulation of R^2.

$$R^2 = 1-\frac{\sum_{i=1}^{m}\sum_{j=1}^{n}\left(I\left(i,j\right)-I'\left(i,j\right)\right)^2}{\sum_{i=1}^{m}\sum_{j=1}^{n}\left(I\left(i,j\right)-\bar{I}\right)^2} \quad (11)$$

In Equation (11), $\bar{I}$ refers to the average of the original image.

SSIM is used to compare the luminance, contrast, and structure of two different images. It can be treated as a similarity measure of two different images. Equation (12) shows the formulation of SSIM.

$$SSIM\left(I,I'\right) = \frac{\left(2\mu_I\mu_{I'}+c_1\right)x\left(2\sigma_{II'}+c_2\right)}{\left(\mu_I^2\mu_{I'}^2+c_1\right)x\left(\sigma_I^2\sigma_{I'}^2+c_2\right)} \quad (12)$$

In Equation (12), μ is the mean intensity, σ is the standard deviation, and c is the constant to avoid instability.

III. EXPERIMENTAL STUDIES

This study modeled 2D shapes in the literature boot, aircraft, cell, pliers, and guitar with IP and signomial functions. In both methods, an additional two layers were created using the 3L method to ensure that the coefficients could express the model effectively. The expression, as well as the number of terms formed due to the degree of power determined for IP, was modeled by the real number of powers of signomial functions. The ABC algorithm was employed to determine the real power degrees of the signomial function. As ABC parameters, the iteration number was selected as 300, the colony size was set at 100, the food source was selected as 50, and the food limit was selected as 25. The study [55] about the performance of the classical ABC algorithm stated that the colony size could be 100. According to the ABC algorithm, the number of food sources is half the colony size. 25 is preferred as the limit value because it is not desired to do too much random search, and it is sufficient considering the preferred value of 300 as the number of iterations. The preferred number of iterations was deemed enough in the preliminary studies, and no improvement was observed in further algorithm execution. As a result of adding the initial power expression of IP stated in Equation (1) as a population element for ABC, thus it increased the sensitivity of the existing model rather than remodeling. From the shapes modeled by experimenting with various order curves: 4, 6, and 8th-degree curves for the Boot picture, 6 and 12th-degree curves for the Aircraft picture, 6, 8, and 10th-degree curves for the Cell picture, 6th-degree curves for the Pliers picture, and 6 and 8th-degree curves for the Guitar picture give better results and these are used.

Figure 1 shows the modeling results of the Boot picture with 4th-degree IP and the signomial function. The signomial function's power degrees are determined with ABC.

When Figure 1 is examined, it is seen that the signomial method with the same degree of power follows the original model better than IP. It is seen that the signomial function modeled with ABC presents more precise modeling success, especially in transition regions and folds.

As shown in Figure 1, ABC could model the curvier area in the right corner and, more precisely, represent the Boot image's base.

The mathematical expression created with ABC for the Boot picture seen in Figure 1 is given in Equation (13).

$$\begin{aligned}
&0.22807\,x^{0.77981}y^{3.368}\\
&\quad+0.22085\,x^{2.0668}y^{4}-1.292\,x^{1.6699}y^{1.5457}\\
&\quad-1.3185\,x^{2.9771}y^{3.3706}-2.0021\,x^{1.1418}y^{1.2684}\\
&\quad+0.022096\,x^{4}y^{3.8223}-0.15188\,x^{1.091}y^{4}\\
&\quad+2.1766\,x^{3.8121}y^{0.84048}+2.4004\,x^{3.452}y^{1.3631}\\
&\quad+7.4518\,x^{1.9107}y^{0.89136}+3.4866\,x^{1.5416}y^{0.4783}\\
&\quad+1.1874\,x^{3.0396}y^{3.2271}-3.2005\,x^{3.8122}y^{1.1727}\\
&\quad-9.0862\,x^{2.2231}y^{0.66466}+0.0218415
\end{aligned} \quad (13)$$

Images of the Boot picture obtained with 6th-degree IP and ABC methods are seen in Figure 2.

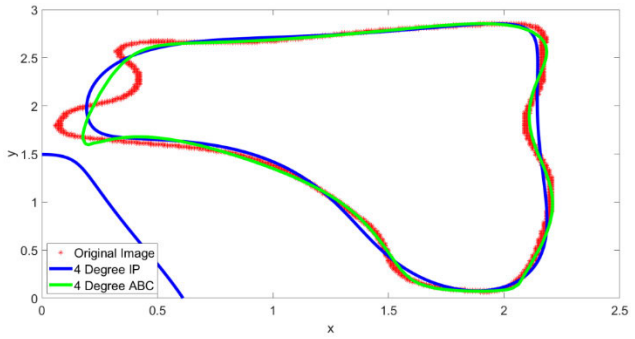

FIGURE 1. Modeling of the Boot picture with 4th degree IP curve and signomial function.

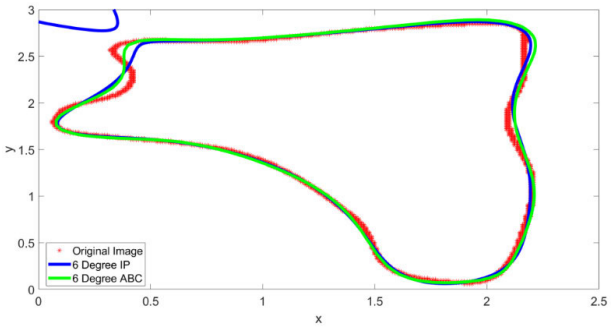

FIGURE 2. Modeling of Boot picture with 6th-degree IP and ABC functions.

As shown in Figure 2, while the bottom of the boot can be modeled at the degree of 6, ABC has again shown more precise modeling success in the left corner, representing the top of the boot. ABC can make more precise curve fitting than IP in the exact order of modeling. Finally, the modeling results and the differences between the Boot picture with 8th-degree IP and ABC modeling are presented in Figure 3.

As shown in Figure 3, while both methods are regarded as successful in 8th-degree modeling, ABC can dig deeper into the curve transition in modeling the upper part of the boot. According to the modeling results, transitions and precision were better in signomial functions established with ABC, especially in low-grade modeling.

The RMSE performance values of the modeling results obtained in Figure 1-3 compared to the original model are shown in Table 2. The RMSE values obtained in Table 2 were calculated according to the estimates of IP and ABC models, with the M value established according to the original model and expressed by Equation (2).

As shown in Table 2, the ABC method has fewer RMSE errors in the modeling performed on the Boot image than IP. Additionally, regarding the error values obtained, the ABC method reduced RMSE error at most at the 4th-degree modeling.

Another image used to test methods in terms of modeling is aircraft, and modeling results of Aircraft picture obtained by the 6th-degree IP and ABC methods are seen in Figure 4.

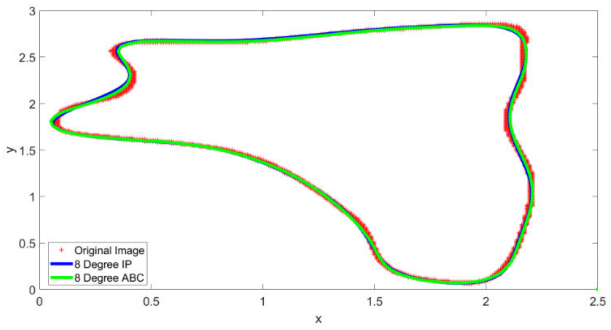

FIGURE 3. The modeling result of the Boot picture was obtained with 8th-degree IP and ABC modeling.

TABLE 2. Performance results of 4th, 6th, and 8th degree IP and ABC modeling of the Boot picture.

Image	Method	RMSE
Boots	4th Degree IP	0.0267
	4th Degree ABC	0.0201
	6th Degree IP	0.0166
	6th Degree ABC	0.0141
	8th Degree IP	0.0110
	8th Degree ABC	**0.0090**

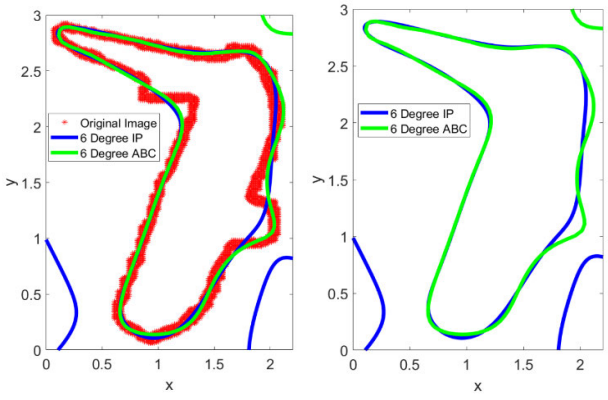

FIGURE 4. Modeling of Aircraft picture with 6th-degree IP and ABC.

As seen in Figure 4, modeling the Aircraft image with ABC at the degree of 6 gives better results than modeling with IP. While primarily in Figure 4, the curved region of the bottom of the aircraft in the right zone can be modeled with ABC, the IP method has passed this region. The RMSE performance values of the modeling results obtained for the Aircraft image compared to the original model are shown in Table 3.

As seen in Table 3, ABC is also more successful in the RMSE error. Successful results have also been obtained in modeling the Cell picture at the degrees of 6, 8, and 10, and modeling results of the Cell picture obtained from the 6th-degree IP and ABC methods are seen in Figure 5.

As shown in Figure 5, the ABC method has also achieved a more successful modeling of the curves that determine the sensitivity. While ABC can model the convoluted transitions

TABLE 3. Performance results of Aircraft picture modeling with 6th and 12th-degree IP and ABC methods.

Image	Method	RMSE
Aircraft	6th Degree IP	0.0173
	6th Degree ABC	0.0163
	12th Degree IP	0.0146
	12th Degree ABC	**0.0135**

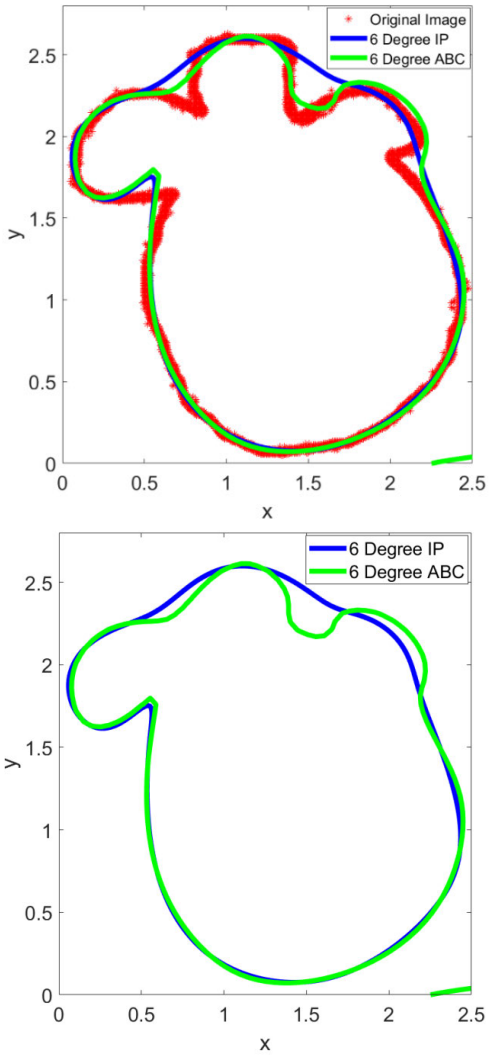

FIGURE 5. Modeling of cell picture with 6th-degree IP and ABC.

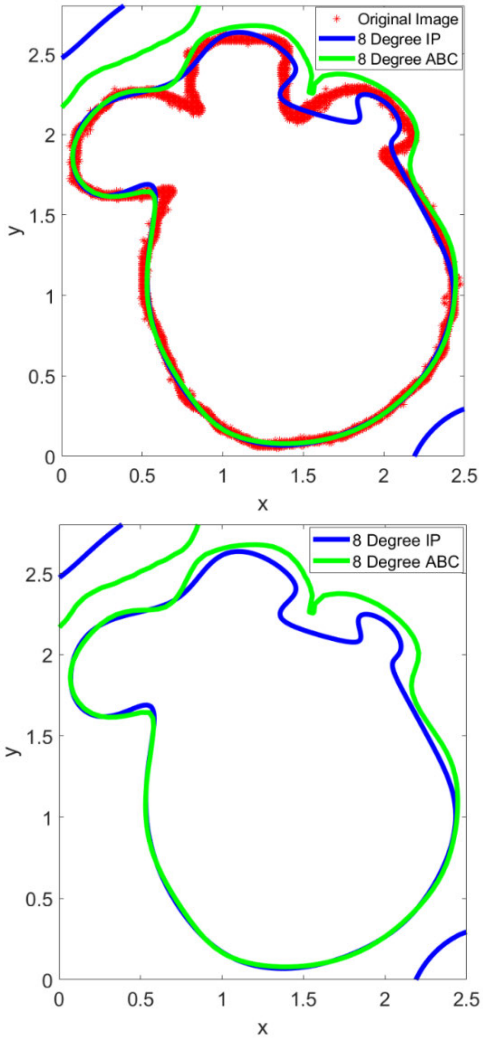

FIGURE 6. Modeling of Cell picture with 8th-degree IP and ABC.

TABLE 4. Cell picture modeling performance results with 6, 8, and 12th-degree IP and ABC methods.

Image	Method	RMSE
Cell	6th Degree IP	0.0186
	6th Degree ABC	0.0164
	8th Degree IP	0.0164
	8th Degree ABC	0.0144
	10th Degree IP	0.0145
	10th Degree ABC	**0.0130**

at the top of the Cell image well, the IP method has passed these regions. The modeling results of the Cell picture obtained from 8th-degree IP and ABC methods are seen in Figure 6.

Successful modeling results were also obtained in Figure 6 using the signomial powers found by the ABC method. Again, the areas with convoluted structures that were challenging to model were modeled more precisely with the ABC method than with IP.

The RMSE performance values of the modeling results obtained for the Cell image compared to the original model are shown in Table 4.

As seen in Table 4, the ABC method has less RMSE value in modeling the Cell image, and higher degree modeling errors with IP can be achieved in the ABC method at lower degrees. The lower degree of modeling allows the mathematical model to be expressed with fewer terms.

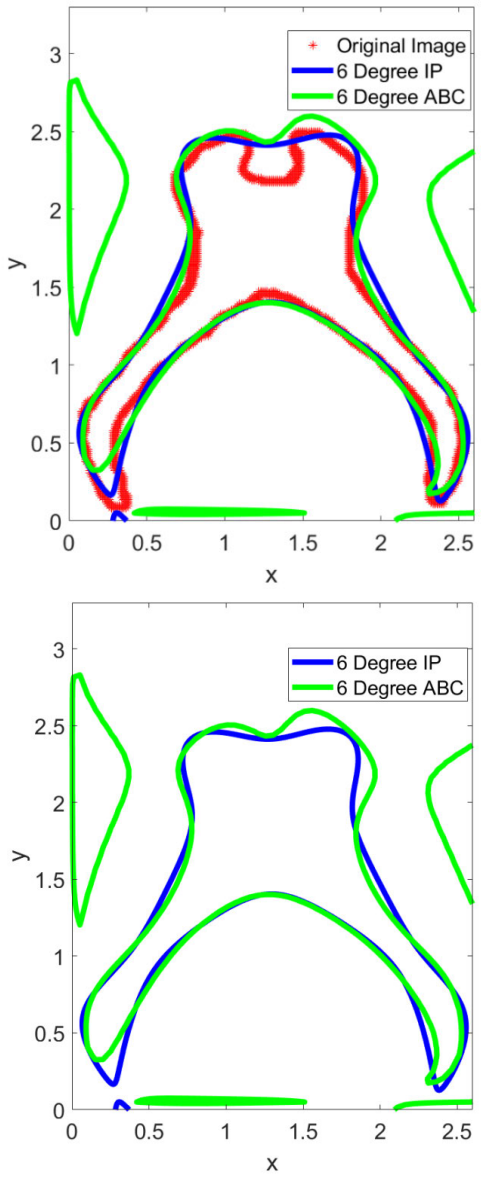

FIGURE 7. Modeling of Pliers picture with 6th degree IP and ABC.

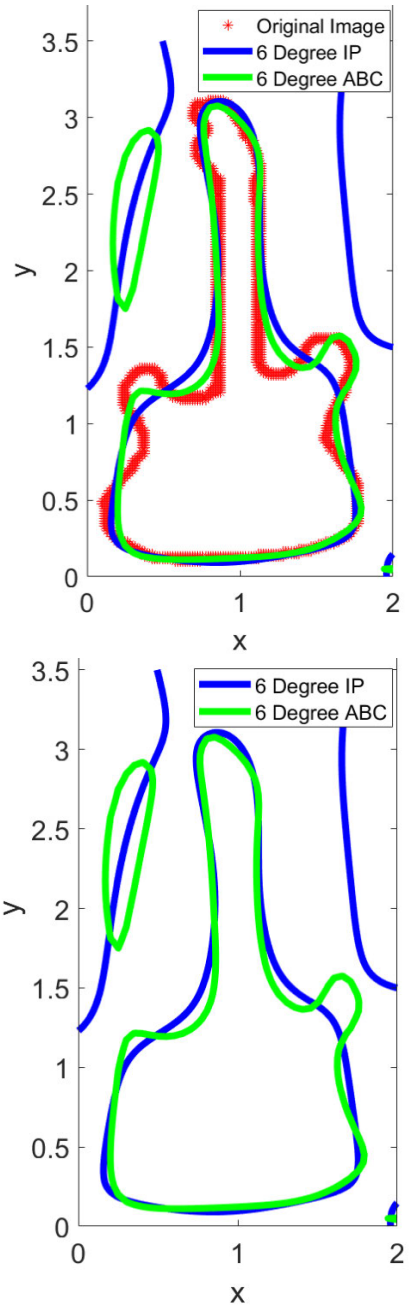

FIGURE 8. Modeling of Guitar picture with 6th degree IP and ABC.

Modeling results of Pliers picture obtained from 6th-degree IP and ABC methods are seen in Figure 7.

As shown in Figure 7, the ABC method can give an indented curve on the top of the Pliers picture, although it is not entirely successful. The IP method has passed this region.

Modeling results of the Guitar picture obtained from 6th-degree IP and ABC methods are seen in Figure 8.

As shown in Figure 8, while the protruding curves on the right and left sides of the Guitar picture are bypassed by the IP method, the ABC method provides the corresponding curve on the right side of these regions. However, the model could not be made up, although a better result was obtained on the left side rather than IP.

Modeling results of the Guitar picture obtained from 8th-degree IP and ABC methods are seen in Figure 9.

When Figure 9 is examined, it is seen that while the ABC method can create a deep curve on the left side, it has successfully been able to model the right area. Although the IP method can form folds at the degree of 8, its results are not seen very well.

The RMSE performance values of the modeling results obtained for Pliers and Guitar images are shown in Table 5 in terms of the original model.

As shown in Table 5, the ABC method has less RMSE value for modeling Pliers and Guitar images and performs more successful modeling than the IP method. When the

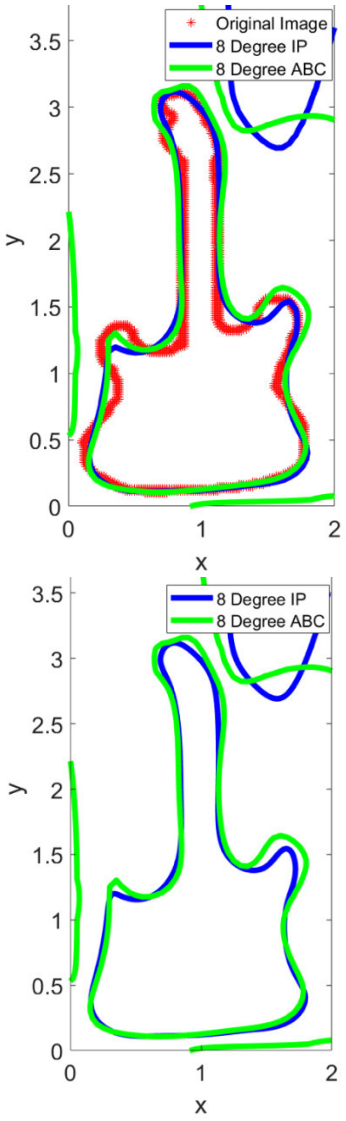

FIGURE 9. Modeling of Guitar picture with 8th degree IP and ABC.

TABLE 5. Performance results of Pliers and Guitar pictures modeling were obtained from 6th and 8th-degree IP and ABC methods.

Image	Method	RMSE
Pliers	6th Degree IP	0.0319
	6th Degree ABC	**0.0231**
Guitar	6th Degree IP	0.0415
	6th Degree ABC	0.0330
	8th Degree IP	0.0322
	8th Degree ABC	**0.0275**

RMSE values obtained on Boots, Aircraft, Cells, Pliers, and Guitar images are considered, the average RMSE values obtained from various levels of modeling on each image are shown in the spider graph in Figure 10.

When Figure 10 is examined, performance values of IP and ABC methods for modeling Boot, Airplane, Cell, Pliers,

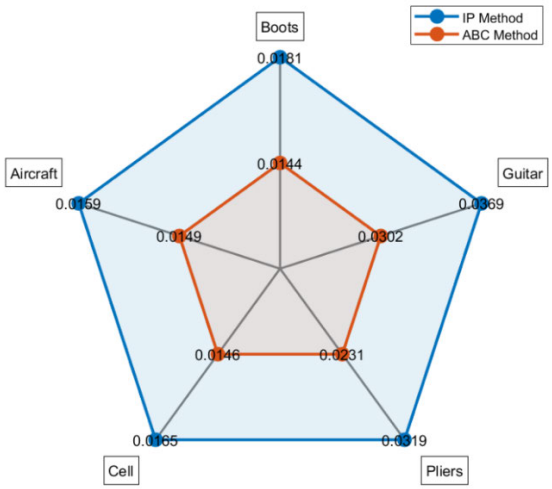

FIGURE 10. The average RMSE values of IP and ABC modeling were obtained on the images.

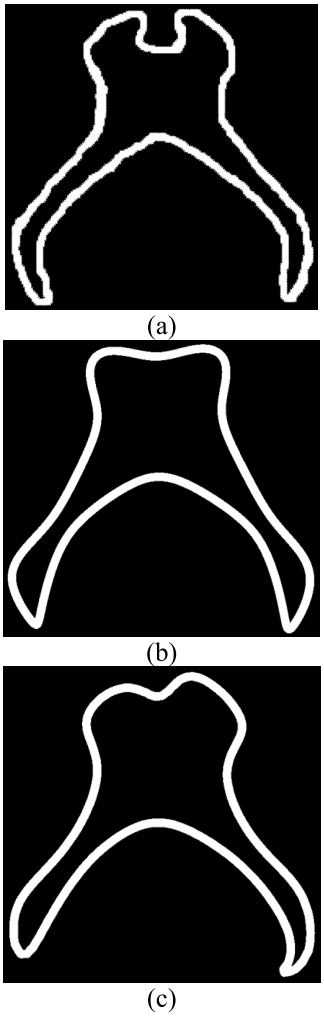

FIGURE 11. Binary Pliers picture, (a) Original Image (b) 6th-degree model with IP (c) 6th-degree model with ABC.

and Guitar images with curves of various orders are seen. When these values are compared, the superiority of the ABC

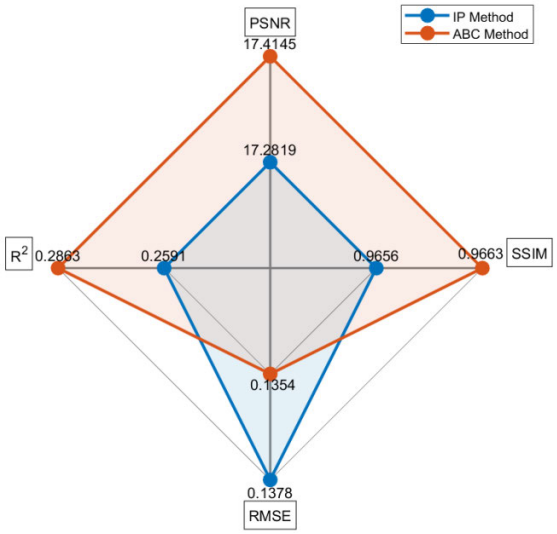

FIGURE 12. The average RMSE, PSNR, R^2, and SSIM values of IP and ABC modeling on the images.

method can be seen when considering the average RMSE values compared to IP. However, another case to consider is that the obtained RMSE values are calculated according to the M value in Equation (2). Only M_0 of the layers specified in the 3L method should be considered when viewed visually. Therefore, the PSNR, SSIM, R^2, and RMSE values, which are popular performance criteria in the literature, were also examined on the images obtained by converting the modeling results to binary images. The RMSE value evaluated in binary images was calculated on the images as the error criterion between the original image and the modeled image.

Even if the IP curves come to a more stable structure with the 3L method, unstable branches can still be seen in regions with zero equality. A simple cleaning method in Algorithm (2) was used to eliminate these unstable branches while obtaining binary images. This means all objects on the binary image are evaluated separately, and all other objects except the largest ones are deleted. The binary images obtained in this way are in the same proportions as the original image in size and are cleaned from the unstable branches. The obtained pictures are now able to perform performance analysis. The image of the Pliers shown in Figure 7 has been transformed into a binary image in Figure 11.

As shown in Figure 11, binary images free of unstable branches and have the same scale are comparable on performance criteria.

The RMSE, PSNR, R^2, and SSIM values obtained from the original binary images of the Boots, Aircraft, Cell, Pliers, and Guitar images and the binary images obtained from the modeling are included in Table 6.

As shown in Table 6, the ABC method can achieve better results in most image and performance criteria. While ABC has achieved more successful modeling in visually complex regions, it has achieved lower values than IP in some performance criteria. However, ABC's superiority over IP, which

TABLE 6. The RMSE, PSNR, R^2, and SSIM values of various degrees of IP and ABC modeling on the images.

Image	Method	RMSE	PSNR (db)	R^2	SSIM
Boots	4th Degree IP	0.1850	14.6584	0.0980	0.9437
	4th Degree ABC	0.1521	16.3561	0.1690	0.9540
	6th Degree IP	0.1429	16.8975	0.2664	0.9559
	6th Degree ABC	0.1483	16.5783	0.2105	0.9541
	8th Degree IP	0.1184	18.5300	0.4963	0.9629
	8th Degree ABC	**0.1123**	**18.9892**	**0.5468**	**0.9644**
Aircraft	6th Degree IP	0.1516	16.3871	0.3530	0.9635
	6th Degree ABC	0.1480	16.5927	0.3829	0.9641
	12th Degree IP	**0.1398**	**17.0909**	**0.4498**	**0.9661**
	12th Degree ABC	0.1445	16.7998	0.4117	0.9652
Cell	6th Degree IP	0.1344	17.4350	0.3403	0.9693
	6th Degree ABC	0.1356	17.3517	0.3275	0.9687
	8th Degree IP	0.1271	17.9189	0.4098	0.9706
	8th Degree ABC	0.1439	16.8386	0.2432	0.9667
	10th Degree IP	0.1281	17.8489	0.4002	0.9706
	10th Degree ABC	**0.1134**	**18.9068**	**0.5299**	**0.9742**
Pliers	6th Degree IP	0.1382	17.1924	0.0612	0.9691
	6th Degree ABC	**0.1340**	**17.4608**	**0.1175**	**0.9699**
Guitar	6th Degree IP	0.1321	17.5819	0.0551	0.9731
	6th Degree ABC	0.1216	18.3024	0.1996	0.9762
	8th Degree IP	**0.1180**	**18.5595**	**0.2456**	**0.9770**
	8th Degree ABC	0.1352	17.3828	0.0108	0.9723

can achieve better results in most criteria than IP, can be seen more clearly when the averages of the relevant performance criteria are considered. Accordingly, the averages of the values obtained in Table 6 are seen in the spider graph given in Figure 12.

Figure 12 shows that the PSNR, R^2, and SSIM average values obtained from the various degrees of the ABC method performed on five different test images are higher and better than those obtained from the IP method. In addition, regarding the RMSE value expressing the error value and expected to be low, ABC again has the advantage over IP.

The results demonstrated that the use of signomial powers increased the modeling success of IP and 3L methods. Furthermore, heuristic methods could be used to detect these powers.

IV. CONCLUSION

Obtain mathematical equation of the objects and their modeling with various methods used in numerical analysis, dynamical systems, chemistry, robotics, reverse engineering of scanned functional surfaces, computer graphics, game and animation, computer-aided design, and modern manufacturing processes. It is vital to perform the modeling accurately and precisely depending on the areas of use. This study attempted to increase modeling success on 2D objects by

using signomial powers and the 3L method for the first time. This approach led to an increase in the success of modeling with the application of signomial functions, as well as an increase in the success of modeling with the existing number of terms. Instead of modeling shapes with higher-order polynomial curves, the shapes were modeled with signomial powers, which provide more precise modeling with the same number of terms. The images of Boots, Aircraft, Cell, Pliers, and Guitar were used in this study. The ABC algorithm was employed to determine these powers, and the average RMSE, PSNR, R^2, and SSIM values were obtained in the order of 0.1354, 17.4145, 0.2863, and 0.9663. These values obtained by the ABC algorithm are more successful than those obtained by the classical IP with the 3L method. It can be seen that modeling success can be increased with signomial powers.

The proposed algorithm is limited in its current form to 2D objects. Its performance should therefore be evaluated initially in the context of modeling and unstable branch removal in 3D objects.

In future work, the signomial powers-based modeling proposed in this study will be employed to enhance the detection of border regions in 3D segmentation of computed tomography images of congenital heart diseases using a deep learning approach such as U-Net. Additionally, a new regression algorithm based on these curves using signomial powers (as well as a binary classification algorithm as in logistic regression) will also be developed.

REFERENCES

[1] G. Taubin, "Estimation of planar curves, surfaces, and nonplanar space curves defined by implicit equations with applications to edge and range image segmentation," *IEEE Trans. Pattern Anal. Mach. Intell.*, vol. 13, no. 11, pp. 1115–1138, Nov. 1991, doi: 10.1109/34.103273.

[2] Z. Lei, M. M. Blane, and D. B. Cooper, "3L fitting of higher degree implicit polynomials," in *Proc. 3rd IEEE Workshop Appl. Comput. Vis. (WACV)*, Dec. 1996, pp. 148–153, doi: 10.1109/ACV.1996.572044.

[3] M. M. Blane, Z. Lei, H. Civi, and D. B. Cooper, "The 3L algorithm for fitting implicit polynomial curves and surfaces to data," *IEEE Trans. Pattern Anal. Mach. Intell.*, vol. 22, no. 3, pp. 298–313, Mar. 2000, doi: 10.1109/34.841760.

[4] K. Kanatani and Y. Sugaya, "Unified computation of strict maximum likelihood for geometric fitting," *J. Math. Imag. Vis.*, vol. 38, no. 1, pp. 1–13, May 2010, doi: 10.1007/s10851-010-0206-6.

[5] J. G. Alcázar and C. Hermoso, "Recognizing projections of algebraic curves," *Graph. Models*, vol. 87, pp. 1–10, Sep. 2016, doi: 10.1016/j.gmod.2016.07.002.

[6] N. Hyodo, Y. Kondoh, H. Murao, T. Saito, and T. Takahashi, "Practice of drawing graphs of implicit functions of three variables," *Commun. JSSAC*, vol. 2, pp. 33–42, Jan. 2016.

[7] M. Fatemi, A. Amini, and M. Vetterli, "Sampling and reconstruction of shapes with algebraic boundaries," *IEEE Trans. Signal Process.*, vol. 64, no. 22, pp. 5807–5818, Nov. 2016, doi: 10.1109/TSP.2016.2591505.

[8] G. Wu and Y. Zhang, "A novel fractional implicit polynomial approach for stable representation of complex shapes," *J. Math. Imag. Vis.*, vol. 55, no. 1, pp. 89–104, May 2016, doi: 10.1007/s10851-015-0615-7.

[9] M. Hasegawa, "Parabolic, ridge and sub-parabolic curves on implicit surfaces with singularities," *Osaka J. Math.*, vol. 54, no. 4, pp. 707–721, 2017.

[10] S. Li, D. Yan, X. Li, A. Hao, and H. Qin, "Hessian-constrained detail-preserving 3D implicit reconstruction from raw volumetric dataset," *Comput. Graph.*, vol. 64, pp. 3–13, May 2017, doi: 10.1016/j.cag.2017.01.001.

[11] S. You and D. Zhang, "Think locally, fit globally: Robust and fast 3D shape matching via adaptive algebraic fitting," *Neurocomputing*, vol. 259, pp. 119–129, Oct. 2017, doi: 10.1016/j.neucom.2016.06.086.

[12] O. Fryazinov and A. Pasko, "Implicit variable-radius arc canal surfaces for solid modeling," *Comput.-Aided Design Appl.*, vol. 14, no. 3, pp. 251–258, Apr. 2017, doi: 10.1080/16864360.2016.1240446.

[13] M. Hu, Y. Zhou, and X. Li, "Robust and accurate computation of geometric distance for Lipschitz continuous implicit curves," *Vis. Comput.*, vol. 33, nos. 6–8, pp. 937–947, Jun. 2017, doi: 10.1007/s00371-017-1370-0.

[14] Y. Song, Y. Luo, Y. Liu, J. Deng, and Z. Yang, "Compression algorithm for implicit 3D B-spline solids," *Commun. Math. Statist.*, vol. 6, no. 2, pp. 119–140, Jun. 2018, doi: 10.1007/s40304-018-0128-y.

[15] T. Tasdizen, J.-P. Tarel, and D. B. Cooper, "Improving the stability of algebraic curves for applications," *IEEE Trans. Image Process.*, vol. 9, no. 3, pp. 405–416, Mar. 2000, doi: 10.1109/83.826778.

[16] T. Sahin and M. Unel, "Globally stabilized 3L curve fitting," in *Proc. Int. Conf. Image Anal. Recognit.*, vol. 3211, 2004, pp. 495–502, doi: 10.1007/978-3-540-30125-7_62.

[17] T. Sahin and M. Unel, "Stable algebraic surfaces for 3D object representation," *J. Math. Imag. Vis.*, vol. 32, no. 2, pp. 127–137, Apr. 2008, doi: 10.1007/s10851-008-0092-3.

[18] Z. Bo, J. Takamatsu, and K. Ikeuchi, "Adaptively determining degrees of implicit polynomial curves and surfaces," in *Proc. Asian Conf. Comput. Vis.*, vol. 4844, 2007, pp. 289–300, doi: 10.1007/978-3-540-76390-1_29.

[19] M. Rouhani and A. D. Sappa, "Relaxing the 3L algorithm for an accurate implicit polynomial fitting," in *Proc. IEEE Comput. Soc. Conf. Comput. Vis. Pattern Recognit.*, Jun. 2010, pp. 3066–3072, doi: 10.1109/CVPR.2010.5540061.

[20] M. Rouhani and A. D. Sappa, "A fast accurate implicit polynomial fitting approach," in *Proc. IEEE Int. Conf. Image Process.*, Sep. 2010, pp. 1429–1432, doi: 10.1109/ICIP.2010.5654043.

[21] M. Rouhani and A. D. Sappa, "Implicit polynomial representation through a fast fitting error estimation," *IEEE Trans. Image Process.*, vol. 21, no. 4, pp. 2089–2098, Apr. 2012, doi: 10.1109/TIP.2011.2170080.

[22] Y. Sato, B. Zheng, Y. Shinya, T. Oishi, and K. Ikeuchi, "Modeling the stone floor based on excavation information using implicit polynomial," in *Proc. 14th IAPR Int. Conf. Mach. Vis. Appl. (MVA)*, May 2015, pp. 65–68, doi: 10.1109/MVA.2015.7153134.

[23] S. Huang, H. Wang, Y. Zhao, and Z. Lin, "An analytical representation of conformal mapping for genus-zero implicit surfaces and its application to surface shape similarity assessment," *Comput.-Aided Des.*, vol. 64, pp. 9–21, Jul. 2015, doi: 10.1016/j.cad.2015.02.002.

[24] J. Rong, S. Yang, X. Mei, X. Ying, S. Huang, and H. Zha, "Ellipse-specific fitting by relaxing the 3L constraints with semidefinite programming," in *Proc. IEEE Int. Conf. Image Process. (ICIP)*, Sep. 2015, pp. 710–714, doi: 10.1109/ICIP.2015.7350891.

[25] J. C. Carr, R. K. Beatson, J. B. Cherrie, T. J. Mitchell, W. R. Fright, B. C. McCallum, and T. R. Evans, "Reconstruction and representation of 3D objects with radial basis functions," in *Proc. 28th Annu. Conf. Comput. Graph. Interact. Techn.*, Aug. 2001, pp. 67–76, doi: 10.1145/383259.383266.

[26] I. Macêdo, J. P. Gois, and L. Velho, "Hermite interpolation of implicit surfaces with radial basis functions," in *Proc. XXII Brazilian Symp. Comput. Graph. Image Process.*, Oct. 2009, pp. 1–8, doi: 10.1109/SIBGRAPI.2009.11.

[27] S. Cuomo, A. Galletti, G. Giunta, and A. Starace, "Surface reconstruction from scattered point via RBF interpolation on GPU," in *Proc. Federated Conf. Comput. Sci. Inf. Syst.*, Sep. 2013, pp. 433–440.

[28] J. Jiao and W. Lingda, "Infrared dim small target detection method based on background prediction and high-order statistics," in *Proc. 2nd Int. Conf. Image, Vis. Comput. (ICIVC)*, Jun. 2017, pp. 53–57, doi: 10.1109/ICIVC.2017.7984517.

[29] H. Zhen-zhong, L. Pei-guo, and M. Jian, "A novel method of extracting and classifying the features of masses in mammograms," in *Proc. 12th Int. Conf. Comput. Sci. Educ. (ICCSE)*, Aug. 2017, pp. 227–231, doi: 10.1109/ICCSE.2017.8085493.

[30] X. Yang and J. Hong, "Dynamic evaluation of free-form curves and surfaces," *SIAM J. Sci. Comput.*, vol. 39, no. 2, pp. B424–B441, Jan. 2017, doi: 10.1137/16m1058911.

[31] S. Cuomo, A. Galletti, G. Giunta, and L. Marcellino, "Reconstruction of implicit curves and surfaces via RBF interpolation," *Appl. Numer. Math.*, vol. 116, pp. 157–171, Jun. 2017, doi: 10.1016/j.apnum.2016.10.016.

[32] W. Zhang and Q. Huang, "Unification of parametric and implicit methods for shape sensitivity analysis and optimization with fixed mesh," *Int. J. Numer. Methods Eng.*, vol. 109, no. 3, pp. 326–344, Jan. 2017, doi: 10.1002/nme.5287.

[33] E. Zieniuk and M. Kapturczak, "Parametric integral equations system in elasticity problems with uncertainly defined shape of the boundary," *AIP Conf. Proc.*, vol. 1863, Jul. 2017, Art. no. 070026, doi: 10.1063/1.4992248.

[34] O. Šedivý, J. M. Dake, C. E. Krill III, V. Schmidt, and A. Jäger, "Description of the 3D morphology of grain boundaries in aluminum alloys using tessellation models generated by ellipsoids," *Image Anal. Stereol.*, vol. 36, no. 1, pp. 5–13, Mar. 2017, doi: 10.5566/ias.1656.

[35] C.-J. Li, L.-L. Xie, and W.-B. Du, "Curve and surface fitting based on the nonhomogeneous linear differential system," *Graph. Models*, vol. 103, May 2019, Art. no. 101026, doi: 10.1016/j.gmod.2019.101026.

[36] R. J. Duffin, E. L. Peterson, and C. M. Zener, *Geometric Programming: Theory and Application*. New York, NY, USA: Wiley, 1967.

[37] P. Shen and K. Zhang, "Global optimization of signomial geometric programming using linear relaxation," *Appl. Math. Comput.*, vol. 150, no. 1, pp. 99–114, Feb. 2004, doi: 10.1016/s0096-3003(03)00200-5.

[38] S.-T. Liu, "A computational method for the maximization of long-run and short-run profit," *Appl. Math. Comput.*, vol. 186, no. 2, pp. 1104–1112, Mar. 2007, doi: 10.1016/j.amc.2006.08.037.

[39] H. Tennakoon and C. Sechen, "Nonconvex gate delay modeling and delay optimization," *IEEE Trans. Comput.-Aided Design Integr. Circuits Syst.*, vol. 27, no. 9, pp. 1583–1594, Sep. 2008, doi: 10.1109/TCAD.2008.927758.

[40] S. Misra, M. W. Fisher, S. Backhaus, R. Bent, M. Chertkov, and F. Pan, "Optimal compression in natural gas networks: A geometric programming approach," *IEEE Trans. Control Netw. Syst.*, vol. 2, no. 1, pp. 47–56, Mar. 2015, doi: 10.1109/TCNS.2014.2367360.

[41] M. M. J. Opgenoord, B. S. Cohen, and W. W. Hoburg, *Comparison of Algorithms for Including Equality Constraints in Signomial Programming*. Cambridge, MA, USA: Massachusetts Institute of Technology, 2017, doi: 10.13140/RG.2.2.13621.78567.

[42] Y. Shen, E. Y. Lam, and N. Wong, "A signomial programming approach for binary image restoration by penalized least squares," *IEEE Trans. Circuits Syst. II, Exp. Briefs*, vol. 55, no. 1, pp. 41–45, Jan. 2008, doi: 10.1109/TCSII.2007.907751.

[43] J. Zhang and W. Ye, "A fast algorithm for binary image restoration," in *Proc. 4th Int. Congr. Image Signal Process.*, vol. 2, Oct. 2011, pp. 590–593, doi: 10.1109/CISP.2011.6100258.

[44] B. Cetisli and H. Kalkan, "Polynomial curve fitting with varying real powers," *Electron. Electr. Eng.*, vol. 112, no. 6, pp. 117–122, Jun. 2011, doi: 10.5755/j01.eee.112.6.460.

[45] P. G. Kirschen, E. Burnell, and W. Hoburg, "Signomial programming models for aircraft design," in *Proc. 54th AIAA Aerosp. Sci. Meeting*, Jan. 2016, pp. 1–27, doi: 10.2514/6.2016-2003.

[46] P. G. Kirschen, M. A. York, B. Ozturk, and W. W. Hoburg, "Application of signomial programming to aircraft design," *J. Aircr.*, vol. 55, no. 3, pp. 965–987, May 2018, doi: 10.2514/1.c034378.

[47] B. Öztürk and A. Saab, "Optimal aircraft design decisions under uncertainty using robust signomial programming," *AIAA J.*, vol. 59, no. 5, pp. 1773–1785, May 2021, doi: 10.2514/1.j058724.

[48] K. Xu, G. Li, K. He, and X. Tao, "Identification of position-dependent geometric errors with non-integer exponents for linear axis using double ball bar," *Int. J. Mech. Sci.*, vol. 170, Mar. 2020, Art. no. 105326, doi: 10.1016/j.ijmecsci.2019.105326.

[49] D. Zhou, E. Pan, and Y. Zhang, "Fractional polynomial function in stochastic response surface method for reliability analysis," *J. Mech. Sci. Technol.*, vol. 35, no. 1, pp. 121–131, Jan. 2021, doi: 10.1007/s12206-020-1211-3.

[50] G. Wang, W. Li, L. Zhang, L. Sun, P. Chen, L. Yu, and X. Ning, "Encoder-X: Solving unknown coefficients automatically in polynomial fitting by using an autoencoder," *IEEE Trans. Neural Netw. Learn. Syst.*, vol. 33, no. 8, pp. 3264–3276, Aug. 2022, doi: 10.1109/TNNLS.2021.3051430.

[51] Y. Tong, L. Yu, W. Li, J. Liu, M. Wu, and Y. Yang, "Mathematical representation of 2D image boundary contour using fractional implicit polynomial," *Optoelectronics Lett.*, vol. 19, no. 4, pp. 252–256, Apr. 2023, doi: 10.1007/s11801-023-2199-6.

[52] R. Interian, J. M. Otero, C. C. Ribeiro, and A. A. Montenegro, "Curve and surface fitting by implicit polynomials: Optimum degree finding and heuristic refinement," *Comput. Graph.*, vol. 67, pp. 14–23, Oct. 2017, doi: 10.1016/j.cag.2017.05.002.

[53] D. Karaboga, "An idea based on honeybee swarm for numerical optimization," Eng. Fac., Comput. Eng. Dept., Erciyes Univ., ayseri, Türkiye, Tech. Rep. TR06, 2005.

[54] D. Karaboga and B. Akay, "A comparative study of artificial bee colony algorithm," *Appl. Math. Comput.*, vol. 214, no. 1, pp. 108–132, Aug. 2009, doi: 10.1016/j.amc.2009.03.090.

[55] D. Karaboga and B. Basturk, "On the performance of artificial bee colony (ABC) algorithm," *Appl. Soft Comput.*, vol. 8, no. 1, pp. 687–697, Jan. 2008, doi: 10.1016/j.asoc.2007.05.007.

IHSAN PENCE was born in Mersin, Türkiye, in 1987. He received the B.S., M.S., and Ph.D. degrees in computer engineering from Süleyman Demirel University, Isparta, Türkiye, in 2010, 2012, and 2016, respectively. Since 2023, he has been the Head of the Software Engineering Department, Burdur Mehmet Akif Ersoy University. He is currently a Faculty Member with Burdur Mehmet Akif Ersoy University. His research interests include optimization, artificial intelligence, pattern recognition, image processing, and deep learning.